# Chirality and domain growth in the gyroid mesophase

By Jonathan Chin and Peter V. Coveney*

*Department of Chemistry, Centre for Computational Science, University College London, 20 Gordon Street, London WC1H 0AJ, UK*

We describe the first dynamical simulations of domain growth during the self-assembly of the gyroid mesophase from a ternary amphiphilic mixture, using the lattice Boltzmann method. The gyroid is a chiral structure; we demonstrate that, for a symmetric amphiphile with no innate preference for left- or right-handed morphologies, the self-assembly process may give rise to a racemic mixture of domains. We use measurements of the averaged mean curvature to analyse the behaviour of domain walls, and suggest that diffusive domain growth may be present in this system.

## 1. Introduction

Emergent phenomena occur when many elements, each with very simple behaviour, display unexpectedly complex behaviour when gathered together in large numbers (Coveney & Skår 2003). Such behaviour gives rise to a vast number of patterns and structures in nature. A good example of this is provided by amphiphile molecules, which, despite having a very simple structure in general, can spontaneously assemble into a wide variety of ordered structures; in particular, the membranes of living cells are constructed from these molecules.

One of these structures is called the gyroid mesophase, whose properties, once assembled, have been studied experimentally and theoretically. However, little is understood about the process of self-assembly. Using a lattice Boltzmann model which can capture both surfactant dynamics and fluid flow effects, we are able to simulate the self-assembly of such a phase. In particular, we demonstrate below that the self-assembly process of the gyroid mesophase can give rise to imperfections or defects in its structure.

## 2. Amphiphile mesophases

The word *amphiphile* comes from the Greek words amfi, for 'both', and filein, 'to like', and means a kind of molecule which is composed of two parts, each attracted to a different species. Soap is a commonly encountered amphiphile: soap molecules are composed of a polar head group which is hydrophilic, or

*Author for correspondence (p.v.coveney@ucl.ac.uk).

1

attracted to water, and a long hydrophobic or lipophilic tail group which is repelled by water and attracted to oil. In a mixture of oil, water and soap, the soap molecules are strongly attracted to the interface between the oil and the water, allowing them to sit in the minimal-energy configuration with the head group facing towards water and the tail group facing into the oil. This tendency to migrate towards interfaces is why such molecules are commonly termed *surfactants*, or surface-active agents. Surfactants have immense industrial importance, mainly due to their tendency to sit at interfaces and thereby reduce surface tension; this is the principle by which all detergents work.

While a solution of surfactant in water is easily prepared in the kitchen sink, such solutions show very rich and complicated behaviour, summarized by, for example, Gompper & Schick (1994) and Langevin (1999), or the reviews of Seddon & Templer (1993, 1995). In a very dilute solution, amphiphile molecules exist as monomers, but beyond a certain critical concentration, they may assemble into a variety of morphologies, such as spherical, wormlike, or branching micellar clusters, or bicontinuous structures, comprised of interpenetrating networks of oil and water channels separated by a monolayer of amphiphile. The networks may be isotropic sponges with no long-range order, but can also form liquid crystalline structures with translational symmetry. This behaviour depends on many variables, such as temperature, surfactant volume fraction, non-polar chain length, polar head-group strength (which, in turn, depends on factors such as pH and ionic concentration) and the form of the interaction between tail groups, between head and tail groups and between head groups.

### ( a )  *The Canham–Helfrich Hamiltonian*

A surfactant molecule in a monolayer will have a variety of lateral forces acting on it. Repulsion between tail groups and between head groups acts to push molecules apart; surface tension effects act to pull them together. The effects of these forces can often be difficult to separate, and the nature of the individual forces is still poorly understood (Seddon & Templer 1995).

A useful idealization of this system is to think of it as being composed of an oil-filled region, a separate water-filled region and a surfactant membrane separating the two. The oil and water regions may have a highly tortuous morphology, giving rise to a correspondingly complicated shape for the surfactant membrane. However, the complicated interactions between molecules can now be described in terms of their net effect on the surface, and, in particular, their effect on its curvature.

Consider a hypothetical symmetric amphiphile, whose head and tail groups are of the same size and exert the same magnitude of forces. At an interface, the ideal configuration of amphiphile molecules is planar; by symmetry, there is no innate preference for the interface to curve in one direction or another. If one bends the surface, then head groups will be pushed together and tail groups pulled apart, or vice versa; this incurs an energy cost. At any point on a surface, maximum and minimum curvatures can be found, corresponding to the minimum and maximum radii of curvature, respectively; the sign of the curvature indicates its direction. These are called the principal curvatures $c_1$ and $c_2$; the mean and Gaussian curvatures are defined as $H = (c + 1 + c_2)/2$ and $K = c_1 c_2$,
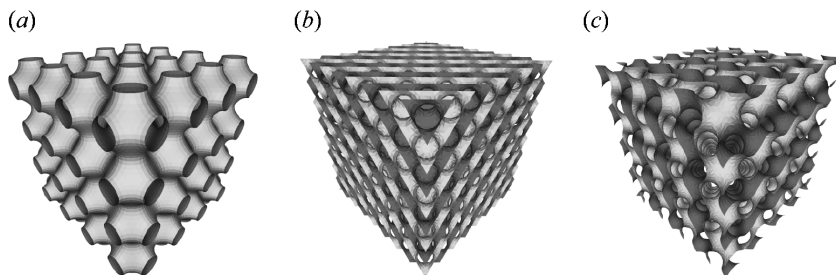
Figure 1. Three common cubic triply periodic minimal surfaces. (*a*) The *P*, or 'plumber's nightmare' surface. (*b*) The *D*, or 'diamond' surface, so called because each labyrinth has the same structure as the carbon atoms in a diamond crystal (Hyde 1989). (*c*) The *G*, or 'gyroid' surface.

respectively. The free-energy cost of curvature at a point on an interface was characterized by Canham and Helfrich (Canham 1970):

$$g_{\mathrm{curv}} = 2\kappa(H - H_0)^2 + \bar{\kappa}K, \qquad (2.1)$$

where $\kappa$ is called the *splay curvature modulus* and $\bar{\kappa}$ is the *saddle splay modulus*. This is integrated over the interfacial surface to find the Hamiltonian for the complete system. The Helfrich Hamiltonian, which describes the energetics of a fictional surface of zero thickness (Schröder *et al.* 2004), is still far from the full story for surfactants; packing frustration and hydrocarbon chain stretching are important, for example, in the inverse hexagonal wormlike micellar phases (Seddon & Templer 1993). However, it is sufficient to predict many of the possible mesophase morphologies.

## (*b*) *Bicontinuous triply periodic minimal surface phases*

The existence of bicontinuous phases was first suggested by Scriven (1976). In these phases, the amphiphile surface must both extend throughout space and minimize its curvature energy. These constraints are satisfied by a class of structures known as triply periodic minimal surfaces (TPMS). A 'minimal surface' has zero mean curvature and negative Gaussian curvature at all points; a TPMS is a minimal surface with cubic symmetry, repeating in the *X*, *Y* and *Z* directions. A brief history of the TPMS is given by Schwarz & Gompper (2002); until 1970, only five TPMS were known, discovered by H. A. Schwarz and his students in the late nineteenth century. Schoen (1970) discovered 12 more, describing them in a NASA technical report. Little attention was paid to the new surfaces, until their existence was rigorously proven by Karcher, who discovered the existence of others in addition (Karcher & Polthier 1996). Further theoretical details of various aspects of periodic minimal surfaces are described in the literature (Mackay 1985; Góźdź & Hołyst 1996; Karcher & Polthier 1996; Klinowski *et al.* 1996; Hyde & Ramsden 2000; Hyde & Schroeder 2003; Lord & Mackay 2003; Enlow *et al.* 2004).

Three surfaces of particular interest in surfactant morphologies are called the *P*, *D* and *G* surfaces (figure 1). *P* and *D* were discovered by H. A. Schwarz; *G*, the 'gyroid', was discovered by Schoen. Fogden & Hyde (1999) give a detailed analysis of the *P*, *D* and *G* surfaces. An analytical form for these three surfaces

(among others) is known in terms of the Enneper–Weierstrass representation (Fogden & Hyde 1999; Gandy & Klinowski 2000), which maps the fundamental patch of each surface into the complex plane. It can be shown (Gandy & Klinowski 2000) that the $P$, $D$ and $G$ surfaces all have the same Weierstrass representation, except for a single parameter $\theta$, called the Bonnet angle. Variation of $\theta$ maps the surfaces on to one another, and is called a Bonnet transformation. The Enneper–Weierstrass representation of these surfaces is unfortunately a little cumbersome to work with, since it involves several elliptic integrals. Nonetheless, it has been used to derive many properties of the surfaces, such as the area, Euler characteristic and Gaussian curvature, per unit cell. These have also been derived numerically for the gyroid and related surfaces of constant mean curvature (Große-Brauckmann 1997), by discretizing a surface and permitting it to evolve, under volume constraints, to $H=0$.

### 3. The gyroid

Of these three surfaces, the 'gyroid' $G$ is perhaps the most interesting. It is the only known TPMS, which is balanced (i.e. the two labyrinths can be mapped onto each other through a Euclidean transformation) while containing no straight lines; it is also the only known TPMS composed entirely from triple junctions. The gyroid has symmetry group $Ia\bar{3}d$; the unit cell consists of 96 copies of a fundamental surface patch, related through the symmetry operations (Gandy & Klinowski 2000) of this space group. Channels run through the gyroid labyrinths in the (100) and (111) directions; passages emerge perpendicular to any given channel as it is traversed, the direction at which they do so gyrating down the channel, giving rise to the 'gyroid' name (Große-Brauckmann 1997). The labyrinths are chiral, so that the channels of one labyrinth gyrate in the opposite sense to the channels of the other. Looking down the (111) direction of a gyroid shows a distinctive 'wagon wheel' pattern (Avgeropoulos *et al.* 1997), which has been observed experimentally in transmission electron micrographs (TEM) of gyroid phases (Shefelbine *et al.* 1999). Gyroids have been observed in many experimental systems, and are usually regarded as the most commonly occurring of the cubic TPMS geometries. They have been seen in triblock copolymers (Shefelbine *et al.* 1999) and lipid–water mixtures (Seddon & Templer 1993, 1995; Mariani *et al.* 1996; Czeslik & Winter 2002). Attempts have been made (Chan *et al.* 1999) to construct a ceramic nanostructured film with the gyroid morphology through the use of a self-assembling polymer template, raising the interesting possibility of fabricating chirally selective porous media. The possibility of using TPMS morphologies for photonic crystals is under active investigation (Urbas *et al.* 2002).

There have been hints that lyotropic liquid crystals may play a part in biological processes such as lipid digestion (Patton & Carey 1979; Rigler *et al.* 1986), and offer insights into cell membrane properties and dynamics (Stier *et al.* 1978; Rand 1981; Prestegard & O'Brien 1987). Donnay & Pawson (1969) suggested that periodic minimal surfaces could be found in nature, and pointed at the microscopic structure of sea urchin skeletons (Nissen 1969) as a possible example; micrographic evidence has since been emerged to suggest that cubic TPMS phases may be present in certain plant cell organelles, and Landh (1995)

suggests, with micrographic evidence, that gyroid structures may exist in the endoplasmic reticulum. Schwarz & Gompper (1999, 2000) examined several TPMS morphologies, and suggested that, for oil–water symmetric systems giving rise to zero spontaneous mean curvature, the gyroid was the most stable structure.

## 4. Dynamical simulations

Despite the significant progress (Schwarz & Gompper 1999) made in free-energy models, which through analysis and Monte Carlo simulation give a good understanding of equilibrium properties and phase stability, comparatively little is known about the dynamics of the cubic phases, or indeed mesophases in general; free-energy functionals will not give information about the dynamics of a system far from equilibrium. The limitation to equilibrium states is a severe one, for several reasons. First, real-world systems may contain boundaries or imperfections, which prevent 'perfect' equilibrium phases from forming. Second, rheological or otherwise dynamical properties of a mesophase are non-equilibrium by definition, and so cannot be captured by such treatments. Many of the mechanical properties of metals and electrical properties of semiconductors are determined primarily by the nature of defects and impurities, so an understanding of the non-equilibrium behaviour is essential for the investigations of material properties. Mesoscale techniques such as dissipative particle dynamics or lattice Boltzmann, since they can handle kinetic descriptions, offer a non-equilibrium alternative to the free-energy descriptions. Q7 Groot & Madden (1998) performed DPD simulations of diblock copolymer melts, which allowed reproduction of several well-known morphologies, and also showed the dynamical pathways through which they were reached. In particular, they showed the existence of a 'gyroid-like' phase with many triple junctions. However, the phase was not exactly of cubic symmetry, possibly because of finite-size effects and frustration.

Using an early version of the LB3D code, Nekovee & Coveney (2001) showed that it was possible to use the lattice Boltzmann model of Chen *et al.* (2000) to simulate the assembly dynamics of lamellar and bicontinuous phases of binary water–surfactant systems; indeed, they showed the existence of a *P*-surface cubic phase of the model. Then, while investigating the effect of the presence of surfactant on spinodal decomposition, González-Segredo & Coveney (2004*a,b*) discovered the existence of a gyroid cubic phase. Importantly, use of the lattice Boltzmann method allowed modelling of the dynamics of the self-assembly of the gyroid. These lattice Boltzmann simulations of the gyroid phase demonstrated several important features. First, it had been suggested (Prinsen *et al.* 2002) that simulation of cubic phases might require a model with more complicated amphiphiles than symmetric dimers, and also that long-range interactions might be required. The lattice Boltzmann simulations, which used symmetric amphiphiles with short-range interactions, refuted this. Second, analysis of the X-ray structure factor of the simulation data showed the existence of oscillating modes at long times; visualization of the simulation output strongly suggested that these were due to Marangoni effects (Scriven & Sternling 1960; Grotberg & Gaver 1996).

Theissen *et al.* (1998) describe a lattice Boltzmann model of amphiphilic systems which is based around a Ginzburg–Landau free-energy functional (Gompper & Schick 1990; Schwarz & Gompper 2000); however, it should be noted that this model lacks an explicit surfactant density, making the assumption that the surfactant is all adsorbed onto the oil–water interface. It is not expected, therefore, that this model would reproduce Marangoni effects at the interface. Lamura *et al.* (1999) describe a Ginzburg–Landau model with explicit surfactant density, but their model, in turn, lacks explicit surfactant orientation. The model used in LB3D has both explicit density and orientation for surfactant particles.

The gyroid self-assembly simulations used initial conditions of a randomized mixture of oil, water and surfactant, with the oil and water in 1 : 1 ratio. Phase separation would occur rapidly, within the first thousand time-steps or so. After phase separation, the system would form a 'molten gyroid' phase, consisting of many oil or water rods surrounded by surfactant; these rods would join up to form triple junctions, giving rise to a gyroid morphology. Towards the end of these simulations, after around 30 000 time-steps, the Marangoni oscillations were observed. These simulations were originally performed to investigate the dynamics of surfactant-limited phase separation; discovery of the gyroid phase was an interesting side effect. Owing to this, the simulations of González and Coveney were not optimally suited to examining the gyroid phase, in several ways. First, they were limited in size: most of the simulation work was done with $64^3$ systems. These are perfectly adequate for phase-separation studies; however, it was observed that while at early times there might be several different gyroid regions with different orientations, at long times these would join up to form a single gyroid grain spanning the entire simulation grid, a so-called 'perfect gyroid'. In the real world, cubic mesophases are far from perfect: despite careful experimental procedures (Hajduk *et al.* 1994), artificially created gyroid materials may not consist of a perfect gyroid repeating throughout space, but rather of many gyroid grains with different orientations. In addition, there may exist dislocations and defects within these grains, analogous to the defects found in ordinary solid crystals (Feynman *et al.* 1964; Kittel 1996). Any investigation of the gyroid domains or the nature of their interactions would require a simulation of sufficient physical size to accommodate several domains for the majority of the simulation.

Second, they were limited in time: the time-scales probed (maximum of 35 000 time-steps) offered few hints as to how transient the effects observed were. Phase separation was observed to happen extremely quickly, over a 1000 time-steps or so, and formation of gyroid morphology on a slower but comparable time-scale. The behaviour of gyroid defects, on the other hand, takes place on a much slower scale, at least tens of thousands of time-steps, and these time-scales were not probed. With these limitations in mind, a new set of simulations was performed specifically to look at the nature of defect dynamics in the gyroid liquid crystal phase.

## 5. The TeraGyroid simulations

It was clear that larger simulations were required; how much larger was not so clear, since defects had not been observed in the unambiguous absence of finite-size effects. Defect dynamics simulations were performed as part of a larger

Table 1. Parameter sets used in TeraGyroid simulations.

| parameter | set 8 | set 9 |
|---|---|---|
| initial oil density $n^{\mathrm{r}}$ | 0.7 | 0.7 |
| initial water density $n^{\mathrm{b}}$ | 0.7 | 0.7 |
| initial surfactant density $n^{\mathrm{b}}$ | 0.9 | 0.6 |
| oil–water coupling $g_{\mathrm{cc}}$ | 0.08 | 0.08 |
| oil–surfactant coupling $g_{\mathrm{cs}}$ | $-0.006$ | $-0.006$ |
| surfactant–surfactant coupling $g_{\mathrm{ss}}$ | $-0.003$ | $-0.0045$ |

Table 2. Simulation durations and end states.

| | system | $t_{\mathrm{max}}$ | output rate $\Delta t$ | final state |
|---|---|---|---|---|
| set 8 | $16^3$ | 5000 | 50 | perfect gyroid |
| | $32^3$ | 50 000 | 500 | perfect gyroid |
| | $64^3$ | 200 000 | 100 | gyroid with dislocation pair |
| | $128^3$ | 384 000 | 250 | single gyroid domain with point defects |
| | $256^3$ | 57 500 | 100 | multiple gyroid domains |
| set 9 | $16^3$ | 5000 | 50 | perfect gyroid |
| | $32^3$ | 100 000 | 500 | perfect gyroid |
| | $64^3$ | 250 000 | 500 | skewed gyroid |
| | $128^3$ | 999 900 | 100 | gyroid with dislocation pair |
| | $256^3$ | 146 500 | 500 | multiple gyroid domains |

project (Pickles *et al.* 2004) to construct a transatlantic distributed simulation grid. As part of this project, a significant amount of computing power became available for use. The simulations of most interest used the parameter sets (González-Segredo & Coveney 2004*a*) called numbers 8 and 9, which are shown in table 1.

Simulations were run at sizes of, among others, $64^3$, $128^3$ and $256^3$, for durations listed in table 2. If a stable gyroid state was reached, then a simulation was terminated; the systems which did not reach this state ran for as long as possible under the resource constraints at the time. During each simulation, the order parameter field $\phi(\boldsymbol{r}) = \rho^{\mathrm{r}}(\boldsymbol{r}) - \rho^{\mathrm{b}}(\boldsymbol{r})$ was stored to disk, as well as the surfactant density field $\rho^{\mathrm{s}}(\boldsymbol{r})$. This was performed every $\Delta t$ time-steps, for values of $\Delta t$ also shown in table 2. The output rate was chosen according to several constraints: it had to be sufficiently rapid to allow observation of the gyroid dynamics, but limits were imposed by local disk quotas, which would often shift due to data from other concurrent jobs.

## 6. Analysis techniques

### (*a*) The structure function

A commonly examined property of mesoscale systems is the *structure function* $S(k)$, defined as the spherically averaged Fourier transform of the order

parameter $\phi(\boldsymbol{r})$:

$$S(k) \doteq \left\langle \left| \int \phi(\boldsymbol{r}) \exp(\mathrm{i}\boldsymbol{k}\cdot\boldsymbol{r}) \mathrm{d}r \right|^2 \right\rangle_{|\boldsymbol{k}'|=k}. \qquad (6.1)$$

This is very closely related to the 'structure factor' measured in small angle X-ray scattering (SAXS) experiments, which are commonly used in experimental examination of mesophases (Avgeropoulos *et al.* 1997; Laurer *et al.* 1997; Sakurai *et al.* 1998; Shefelbine *et al.* 1999), and has been an important tool in the analysis of many mesoscale simulations (Velasco & Toxvaerd 1993; Rybka *et al.* 1995; Wagner & Yeomans 1998; González-Segredo & Coveney 2004*b*). To measure the dominant length-scale of a system, the reciprocal space first moment $k_1$ of $S(k)$ is usually calculated:

$$k_1 \doteq \left( \int k S(k) \mathrm{d}k \right) \Big/ \left( \int S(k) \mathrm{d}k \right). \qquad (6.2)$$

The corresponding length-scale is then $L_1 \doteq 2\pi/k_1$.

### (*b*) *Polygonal approximation of the interface*

Since the interfacial properties are so crucial to the behaviour of the gyroid phase, it is important to be able to extract the location of the two-dimensional interfacial surface from the three-dimensional simulation data. In a continuum system, the interface between the oil and water phases can be defined as the implicit surface $\phi(\boldsymbol{r}) = \rho^{\mathrm{r}}(\boldsymbol{r}) - \rho^{\mathrm{b}}(\boldsymbol{r}) = 0$, for $\boldsymbol{r} \in \mathbb{R}^3$. In contrast, the simulation output data consists of the values of $\phi$ at discrete sites $\boldsymbol{r}_i$ on the lattice; it is not quite so straightforward to define an interfacial surface because, in general, while $\phi(\boldsymbol{r}_i)$ can be positive or negative, corresponding to the lattice site containing a majority of red or blue particles, respectively, it is almost never exactly zero. However, a continuum order parameter field can still be estimated from the discrete simulation output, by linear interpolation; this interpolated function is single-valued and continuous across the simulated region, and can be regarded as the simulated approximation to the order parameter field; the isosurface $\phi^{\mathrm{interp}}(\boldsymbol{r}) = 0$ is then well defined.

Generation of a polygon mesh approximation to this surface can be achieved through several means. The most popular method is known as marching cubes: this technique was developed by Lorensen & Cline (1987). In marching cubes, each point $\boldsymbol{r}$ on the lattice is assigned a value of 1 if $\phi(\boldsymbol{r})$ is 'negative', or unambiguously less than zero, and 0 if $\phi(\boldsymbol{r})$ is 'positive', i.e. greater than zero or within floating-point error of zero. If a positive site is adjacent to a negative site, then $\phi(\boldsymbol{r})$ changes sign somewhere along the link between the two sites, and therefore the link between the sites intersects the contour surface; the position of these intersections can be found easily through interpolation. The marching cubes algorithm proceeds by considering each cube of eight sites in turn, calculating a number between 0 and 255, representing the state of these sites, and then using this number to find a set of polygons approximating the interface shape inside the cube. The polygon sets can be stored in a lookup table, making the algorithm extremely fast.

Unfortunately, the algorithm is not guaranteed to produce a surface with the same topology as the implicit interpolated surface $\phi^{\mathrm{interp}} = 0$. In fact, it is possible for marching cubes to produce 'non-manifold' surfaces containing holes; this

arises because some of the 256 possible states of a cube have more than one way of being tiled with polygons, and the tilings are topologically different.

Several approaches have been suggested to correct this problem. One such technique is to tile the space with tetrahedra rather than cubes (Carneiro *et al.* 1996; Treece *et al.* 1999), which produces a topologically consistent surface without holes, but at the expense of speed, memory and geometrical accuracy (Lewiner *et al.* 2003). Another approach is the recursive dividing cubes algorithm (Cline *et al.* 1988), which has similar performance penalties, particularly for large datasets.

Chernyaev (1995) observed that it was possible to extend the marching cubes approach to produce polygon surface meshes which are not only topologically consistent (i.e. do not have any holes), but also topologically correct (i.e. homeomorphic to the surface $\phi^{\mathrm{interp}} = 0$). An implementation of this technique was described by Lewiner *et al.* (2003), who used lookup tables to determine which tests to perform, resulting in a very efficient algorithm to produce a triangle mesh which is both topologically consistent and topologically correct.

### (c) Fluid properties at the interface

By applying this algorithm to the simulation output datasets, a polygonal approximation to the interface between the two fluid components can be found. This is useful not only for direct visualization of the system, but also for calculating many interesting properties.

First, the interfacial area of the system can be calculated, simply by adding up the areas of all of the triangles in the surface. Without knowing the location of the interface, any space-varying property $\alpha(\boldsymbol{r})$, such as surfactant density, can only be averaged over the bulk of the three-dimensional system. However, once the interface has been polygonized, the variation of $\alpha$ over the interface can now be found, by interpolating $\alpha$ to the surface vertices and taking an area-weighted average. Consider a single triangle $\boldsymbol{\Delta}_i$, area $A_i$, vertices $\boldsymbol{a}_i, \boldsymbol{b}_i, \boldsymbol{c}_i$. The value of $\alpha$ averaged over the triangle is

$$\alpha_i = \frac{1}{A_i} \int_{\Delta_i} \alpha(\boldsymbol{r}) \mathrm{d}^2 A_i \simeq \frac{1}{3}[\alpha(\boldsymbol{a}_i) + \alpha(\boldsymbol{b}_i) + \alpha(\boldsymbol{c}_i)]. \qquad (6.3)$$

This relationship is exact if $\alpha$ varies linearly over the surface of the triangle. Integrating $\alpha$ over the entire closed polygon mesh $M$ is equivalent to summing the values integrated over each individual triangle:

$$\oint_M \alpha(\boldsymbol{r}) \mathrm{d}^2 A = \sum_i \int_{\Delta_i} \alpha(\boldsymbol{r}) \mathrm{d}^2 A_i \simeq \sum_i \alpha_i A_i. \qquad (6.4)$$

Hence, the average of $\alpha$ over the surface is

$$\langle \alpha \rangle_M = \frac{\sum_i \alpha_i A_i}{\sum_i A_i}. \qquad (6.5)$$

### (*d*) *Interfacial curvature*

Any point $\boldsymbol{r}$ on the surface $\phi(\boldsymbol{r}) = 0$ has a unit normal $\hat{\boldsymbol{n}}$, defined as $\hat{\boldsymbol{n}}(\boldsymbol{r}) \doteq (\nabla\phi)/|\nabla\phi|$. The shape operator $\mathbb{S}$ is a rank-2 tensor defined as $\mathbb{S} \doteq -\nabla\hat{\boldsymbol{n}}$.

The Gaussian and mean curvatures can then be found from the determinant and half the trace of the shape operator, respectively. More usefully, the surface-averaged value of the squared mean curvature, $\langle H^2 \rangle_{\mathrm{surf}}$ can also be calculated; this quantity is physically interesting because it appears as a term in the Helfrich Hamiltonian. The contribution to the surface-averaged curvature from each lattice site can also be calculated. This curvature field has low values where there is no interface, or where the interface has a minimal surface structure, and it has a high value where the interface is highly curved; consequently, it can be used to distinguish non-minimal-surface defect regions from the bulk gyroid phase (figure 5).

### (*e*) *Interfacial Euler characteristic*

Consider a two-dimensional closed surface tiled with a polygon mesh; each polygon is joined to its neighbours by a straight edge, and the edges meet at point vertices. Suppose that the surface has $V$ vertices, $E$ edges and $F$ polygon faces; the Euler characteristic or Euler number of the surface is defined as $\chi^{\mathrm{surf}} \doteq V - E + F$. A surprising and very powerful result of elementary topology (Kinsey 1993; Nakahara 1993; Armstrong 1997) is that the Euler characteristic depends only on the topology of the surface, and not on its shape or the manner in which it is tiled with polygons. More precisely (Kinsey 1993), if $S_1$ and $S_2$ are compact, connected surfaces without boundary, then $S_1$ is topologically equivalent to $S_2$ if and only if $\chi(S_1) = \chi(S_2)$, and either both are orientable or both are non-orientable. A surface is non-orientable if it contains Möbius bands; all of the surfaces under consideration here are orientable, so determination of topological equivalence reduces to comparison of the Euler characteristic.

The Euler number is additive; a system with $n$ surfaces $S_i$ each with Euler number $\chi_i$ has total Euler number $\sum_i \chi_i$. The surface meshes produced by the marching cubes algorithm are composed entirely of triangles; this property simplifies calculation of the Euler characteristic. Each triangle on the mesh has three edges; each edge on the mesh joins exactly two triangles. Hence, the number of edges is $3/2$ times the number of triangles: $\chi^{\mathrm{tri}} = V - E + F = V - (1/2)F$.

The Euler number of a surface is directly related to another topological quantity called the genus $g$, which is often regarded as simply the number of holes in the surface. For an orientable surface (Kinsey 1993), $\chi = 2(1 - g)$. The Euler number is an extremely useful concept when trying to understand the output of mesoscale simulations. Imagine a lattice Boltzmann simulation of a spherical-droplet phase, where the droplets are defined as regions for which the order parameter $\phi(\boldsymbol{r}) < 0$. Since the Euler number of a sphere is 2, and since it is additive, the number of droplets in the system is simply half the Euler number of the $\phi = 0$ surface. Moreover, the Euler number, being a topological invariant, is insensitive to fluctuations in the droplet shape or size, provided that each droplet remains simply connected.

Recently, the Euler number was used by Hołyst & Oswald (1998) to characterize fluctuating wormhole-like passages (Goos & Gompper 1993) appearing in Monte Carlo simulations of lamellar phases; similar wormholes

491    have been observed in a lattice gas dynamical model (Boghosian *et al.* 1996). In a
492  Q8  system with periodic boundary conditions, a membrane spanning both the $x$ and
493    $y$ directions is topologically equivalent to the surface of a torus, and therefore has
494    Euler number zero; thus, a lamellar stack of membranes will also have Euler
495    number zero. However, if a wormhole forms between two lamellae, the Euler
496    number will suddenly jump to $-2$, hence the Euler number is $-2n$ for $n$ such
497    wormholes. The Euler number has also been used in examinations of TPMS
498  Q9  surfactant morphologies (Schwarz & Gompper 2000) and experimental MRI data
499    (Gerig *et al.* 1999). A gyroid surface has Euler characteristic $-8$ per unit cell.

## 7. Analysis of the simulation data

504    So far, both the techniques used to simulate assembly of the gyroid mesophase
505  Q10  and the techniques used to analyse the resulting data have been presented. The
506    following section presents the actual analysis of the generated data, and a
507    discussion of the physics involved.

### (a) Initial phase separation

510    The simulated system is initialized to a very highly mixed and disordered
511    state, often called a 'quench' in the literature. The system undergoes spinodal
512    decomposition (Bray 1994; Kendon *et al.* 1999; Chin & Coveney 2002;
513    González-Segredo *et al.* 2003), and rapidly divides into interpenetrating regions
514    of bulk water and bulk oil, separated by a layer of surfactant. If the system
515    contained only water and oil, each component would eventually form a single
516    large domain; however, this situation would leave insufficient surface area to
517    allow all of the surfactant to sit at the oil–water interface. Therefore, the
518    surfactant has the effect of limiting the domain growth (Love *et al.* 2001).
519    Figure 2 shows the dominant length-scale $L_1(t)$ for the first 5000 time-steps of
520    three simulations using parameter set 8. This shows that the length-scale rapidly
521    increases as the oil and water components separate, but stays relatively constant
522    after around 1000 time-steps. Figure 3 shows renderings of the oil–water interface
523    at $\phi=0$ over the first 500 time-steps, indicating that the rapid increase in
524    structure factor corresponds to the formation of a mesh of interconnecting
525    channels, all of roughly the same width. Visual inspection of the interface shows
526    that no gyroid structure is present during the channel formation.

### (b) Gyroid formation: parameter set 9

530    Figure 4 shows the mean curvature $H$ of the $\phi=0$ interface, averaged over the
531    whole surface. The most obvious feature of this graph is the magnitude of the
532    curvature fluctuations in each system. The $256^3$ system, being the largest, had
533    the most interfacial area over which to average: $\langle H \rangle$ therefore had the lowest
534    amount of fluctuation in this system, with a standard deviation of $8.41 \times 10^{-5}$
535    inverse lattice units. The $128^3$ system had fluctuations roughly twice as large,
536    with a standard deviation of $1.70 \times 10^{-4}$, and the $64^3$ a little over twice as large
537  Q11  again, at $3.86 \times 10^{-4}$ inverse lattice units (figure 5).
538    The next obvious feature of figure 4 is that, while the $128^3$ and $256^3$ systems
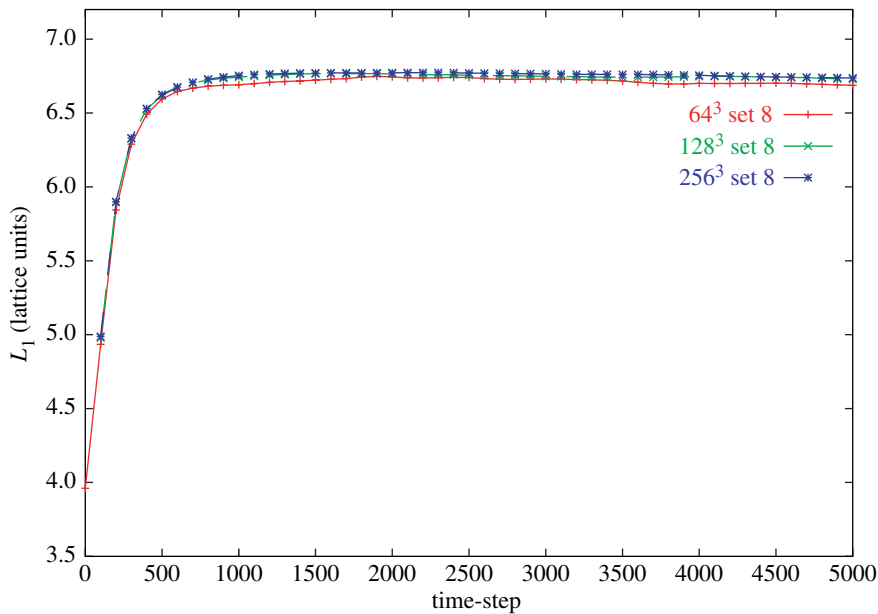539    fluctuated about zero for the entire simulation duration, the $64^3$ simulation

Figure 2. Typical length-scale $L_1(t)$ as a function of time, for three simulations on parameter set 8.

dropped to a negative-mean-curvature geometry after around $10^5$ time-steps. Visual inspection showed that this corresponded to the system collapsing into a stable state, forming a regular structure which filled the entire simulation lattice, apart from two point defects.

Looking along the $Y$-axis, the structure reconnected with itself through the periodic boundary conditions, moving half a unit cell in each of the $X$ and $Z$ directions after traversing the lattice. There were seven unit cells in the $X$ and $Z$ directions, and six and a half in the $Y$ direction; a topologically perfect gyroid with this many unit cells would have an Euler characteristic of $-2548$. The simulated structure had $\chi = -2540$ due to the presence of the point defects. The skewing of the 'gyroid' in the $X$ and $Z$ directions and consequent rhombohedral (rather than cubic) liquid crystal structure meant that the oil–water interface did not form a zero-mean-curvature gyroid structure, but a skewed gyroid with, on average, negative mean curvature. It should be noted that the production of a gyroid with this orientation is a reassuring sign that the production of a gyroid mesophase is not a simulation artefact due to some anisotropy induced by the lattice, in which case such misalignment would not be expected.

Figure 6 shows the $\phi = 0$ isosurface, coloured red on the oil-majority side and blue on the water-majority side, at time-step $2.5 \times 10^5$. The region shown lies at the interface between the two domains; the domain wall is shown running vertically through the centre of the diagram. Careful examination of the channels running through the diagram shows that, while the two domains contained gyroids with roughly the same orientation, the domains had opposite chirality: red channels spiral clockwise away from the viewer in the right-hand side domain, but anticlockwise away from the viewer in the left-hand side domain. Since the model used is oil–water symmetric, there should be no preference for, say, oil channels to be left-handed, so the existence of chiral domains is to be expected.
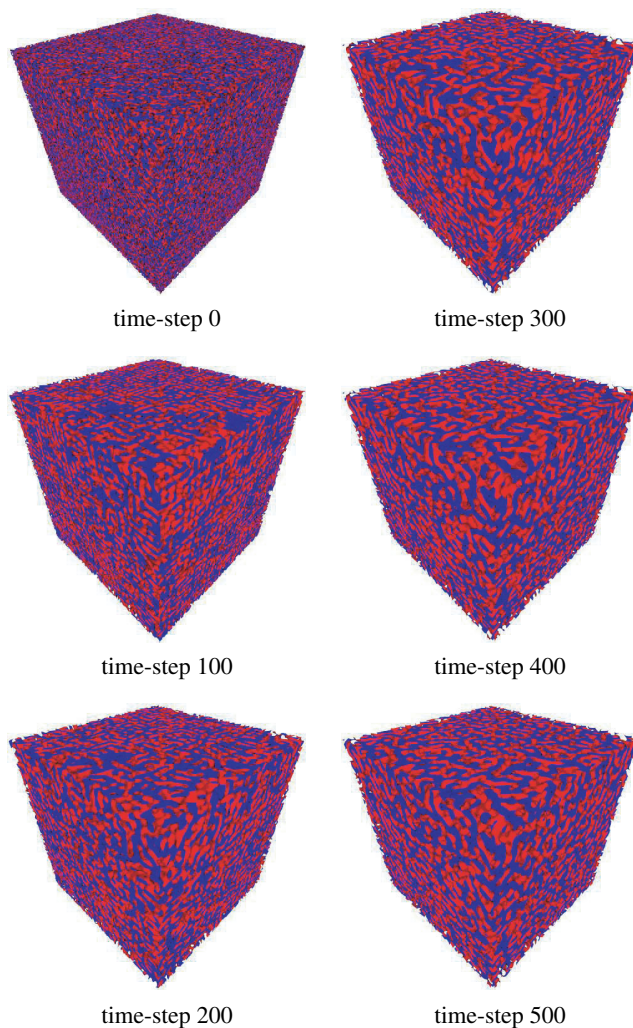
589
590
591
592
593
594
595
596
597
598
599
600
601
602
603
604
605
606
607
608
609
610
611
612
613
614
615
616
617
618
619
620
621
622
623
624
625
626
627
628
629
630
631
632
633
634
635
636
637



Figure 3. The oil–water interface ($\phi=0$) during early time evolution of a parameter set 8 system running on a $128^3$ lattice.

Figure 5 shows volume renderings of the curvature contribution, highlighting regions with high interfacial curvatures. At time-step 10 000, the gyroid structure had not emerged, but by time-step 40 000, multiple gyroid domains were visible. These domains were observed to merge, until only two domains were left in the system, around time-step 200 000. One of the domains then collapsed over the next hundred thousand time-steps, leaving behind two columnar defect regions which persisted for as long as the simulation continued.

Figure 7 shows a volume rendering of the order parameter field at time-step $5\times10^5$, with the transfer function chosen to highlight regions of high oil density and regions of high water density in red and blue, respectively. By this time, the domain walls had collapsed into a pair of dislocation lines running right through
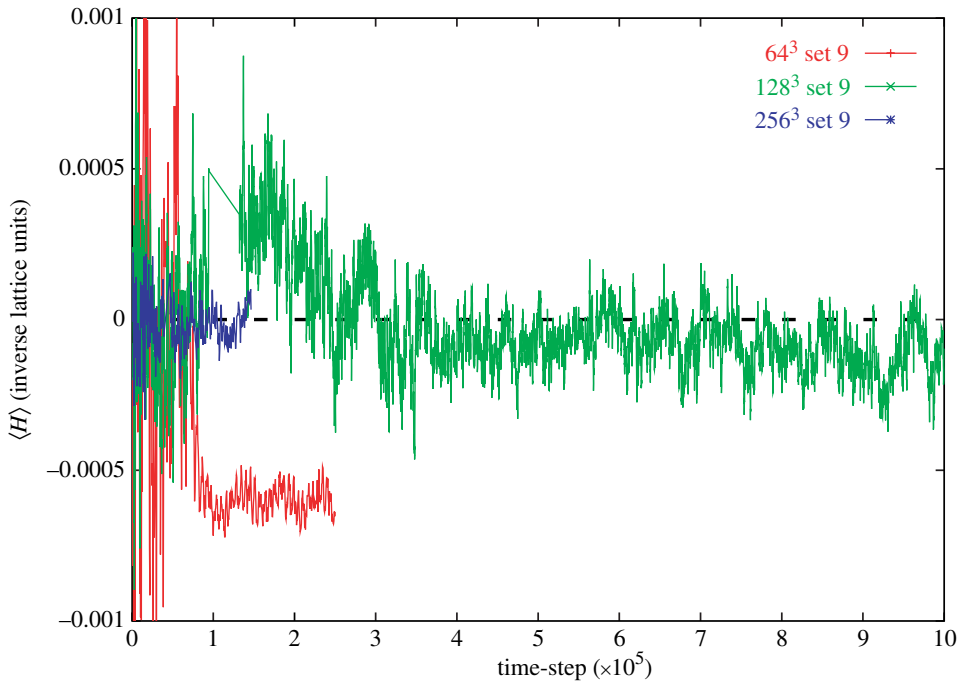
Figure 4. Mean curvature $H$ averaged over the $\phi=0$ surface for parameter set 9, for three different simulation lattice sizes.

the system. The green lines show a Burgers loop (Kittel 1996) around each dislocation; it can be seen that the Burgers vectors for each dislocation are equal in magnitude and opposite in direction (figures 8–10).

### (c) Gyroid formation: parameter set 8

Figures 11 and 12 show the surface-averaged mean curvature $\langle H \rangle$ and surface-averaged squared mean curvature, respectively, for simulations using parameter set 8. The fluctuations in the mean curvature again dropped in magnitude with increased system size, just as observed with parameter set 9. On closer examination, the fluctuations for the $128^3$ simulation dropped in magnitude around time-step $2.5\times10^5$, with a similar halt in the evolution of the other bulk and interface properties. The domain wall visualizations (figure 13) show that the system produced two domains at late times, and one of these disappeared around time-step $2.5\times10^5$, leaving no dislocations or other major defects in the system. It was verified by direct inspection that the last two domains were again of opposite chirality. At the end of the simulation, time-step 378 500, the system was found to contain a gyroid with 15 unit cells in each direction, with an Euler characteristic of $-26\,828$, corresponding to 3353.5 gyroid unit cells. A $15^3$ periodic gyroid would be expected to contain 3375 unit cells; the discrepancy is attributed to persistent point defects, which appeared as the domains formed, up to time-step $10^5$, and remained unchanged for the rest of the simulation.

The $256^3$ simulation, limited only by available computer time, ran until time-step 57 500, at which point it was still composed of multiple chiral gyroid
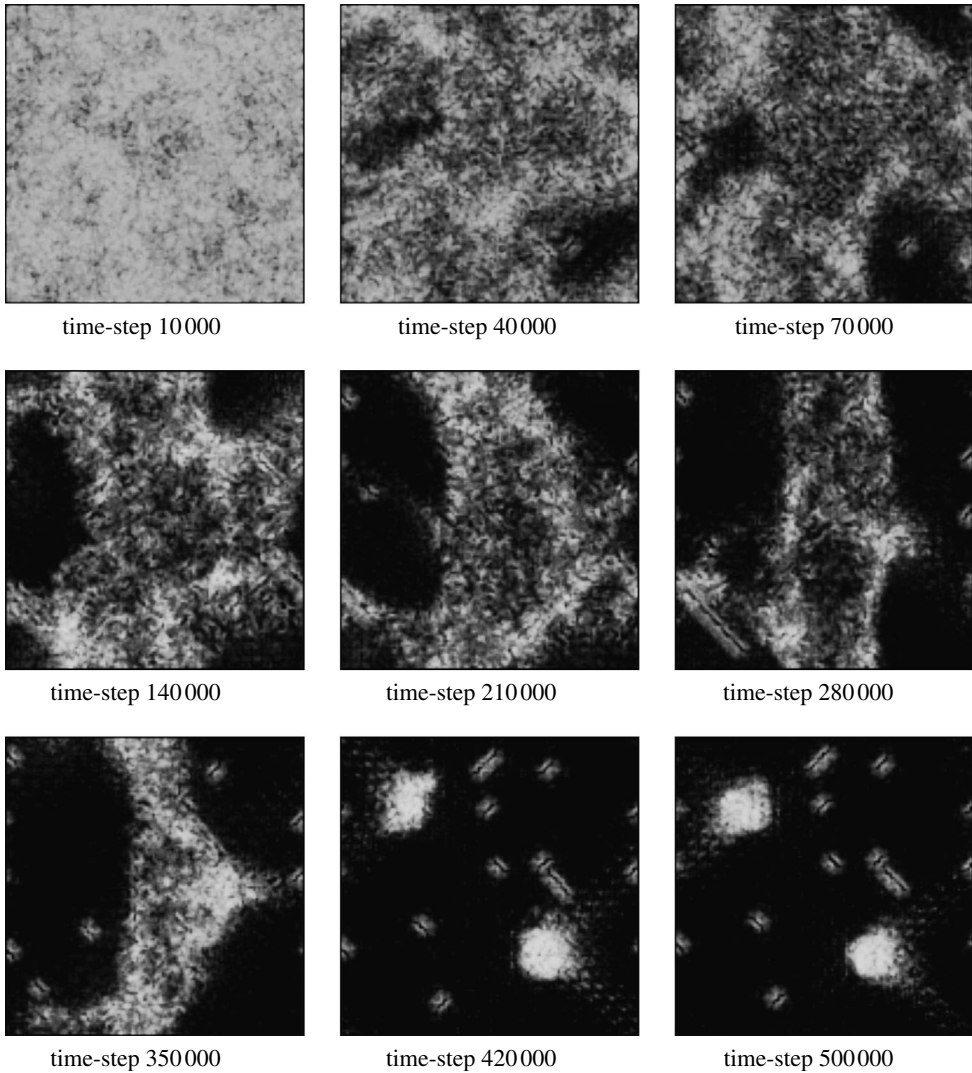
687
688
689
690
691
692
693
694
695
696
697
698
699
700
701
702
703
704
705
706
707
708
709
710
711
712
713
714
715
716
717
718
719
720
721
722
723
724
725
726



Figure 5. Orthographic-projection volume rendering highlighting domain walls for a $128^3$ simulation using parameter set 9, showing the late-time collapse of the last domain into a pair of line dislocations. Periodic boundaries are enforced; one of the dislocations straddles an edge of the simulation box.

domains. The domains were observed to interpenetrate in a manner not unlike the morphology of single-component fluid domains during spinodal decomposition.

Figure 8 shows the averaged squared mean curvature plotted against time for
Q13 $128^3$ and $256^3$ simulations of parameter sets 8 and 9. Both of the parameter set 8 systems appeared to take on fairly close power-law behaviour (seen as straight lines on the log–log graphs) after time-step $10^4$, when the system recognizably contained gyroid regions. The parameter set 9 systems also did this, but took longer to do so; the value of $\langle H^2 \rangle$ for the set 9 systems was somewhat larger than
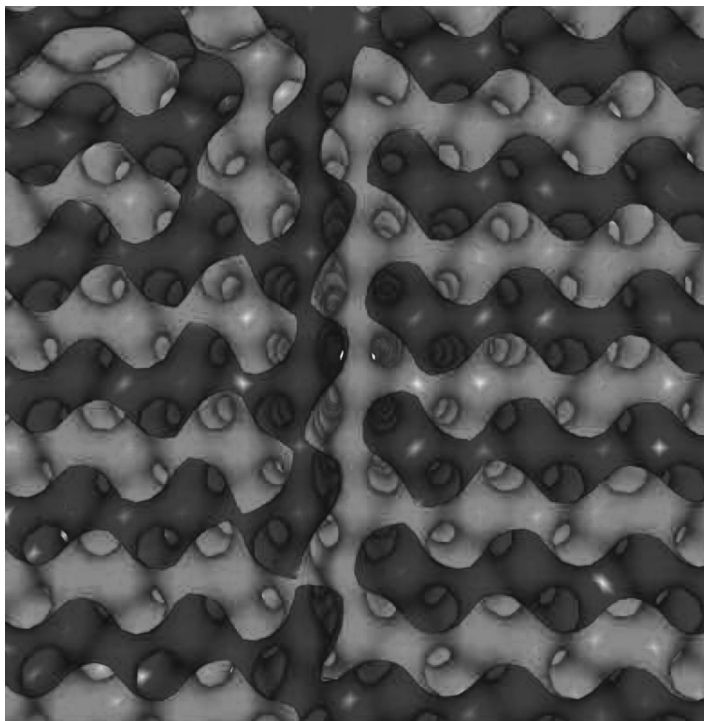
Figure 6. The oil–water interface at time-step $2.5 \times 10^5$ for the $128^3$ simulation of parameter set 9. Note that the domains have opposite chirality.

that of the set 8 systems, until around time-step $5 \times 10^4$, at which point they appeared to show the same behaviour. The $128^3$ systems eventually deviated from the power-law behaviour as finite-size effects set in, around time-step $2 \times 10^5$ for set 8 and $3 \times 10^5$ for set 9.

Figure 10 shows renderings of the domain walls and defects of the parameter set 9 system at points before and just after it reached power-law behaviour, with the defects for the parameter set 8 system plotted for comparison. During the period when the set 8 system showed power-law scaling but the set 9 system did not, the latter appeared to have a rather higher density of defective regions, shown as dark regions in the volume renderings. After time-step 50 000, both systems appeared clearly separated into domains.

The datasets for $\langle H^2 \rangle(t)$ for each simulation were trimmed to only include the time-steps after 10 000, when gyroid structures form, for the parameter set 8 simulations, and the time-steps after 50 000, after clear domain formation, for the parameter set 9 simulations; they were also restricted to the time-steps before the sudden drop in and stabilization of the squared mean curvature for the $128^3$ simulations, to exclude the corresponding finite-size effects.

A relation of the form $\langle H^2 \rangle = at^n$ was then fitted to each trimmed dataset; the fitted values of the exponent $n$ are given, along with the relevant time periods, in table 3. The fitted exponents together had a mean of $-0.481$ and standard deviation of 0.037. This is quite close to an exponent of $n = -1/2$; the data points
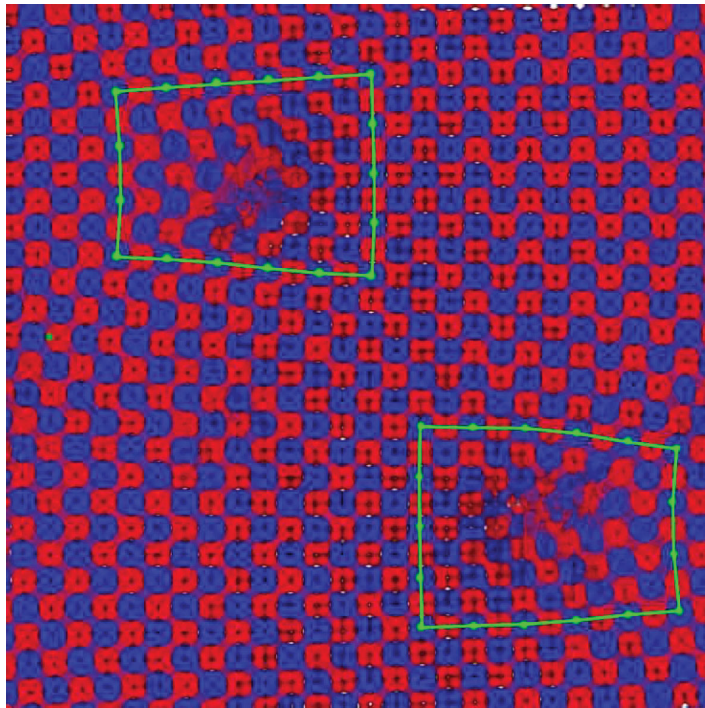
Figure 7. Orthographic-projection volume rendering of the $128^3$ simulation of parameter set 9 at time-step $5 \times 10^5$. Oil-bearing regions are highlighted in red, water-bearing regions in blue and the interfacial regions are suppressed. The green lines show Burgers circuits around the two dislocations.

to which these fits were made are plotted together in figure 8, along with a $t^{-1/2}$ power law for comparison. A possible reason for power-law scaling and for why the exponent should be $-1/2$ is given below.

Consider a large system of volume $V$, containing many gyroid domains. Let the length-scale of a typical single domain be $L_1(t)$, and suppose that the gyroid length-scale grows as a power law of time, $L_1 \sim t^n$, just as domains often do in, e.g. spinodal decomposition. The surface area of a single domain will then scale as $A_1 \sim t^{2n}$, and the volume of a single domain as $V_1 \sim t^{3n}$.

The total number $N$ of domains in the system is $V/V_1$, so $N \sim t^{-3n}$. The total surface area $A$ of domains is proportional to both the number of domains and the typical surface area of a single domain, so therefore $A \sim t^{-n}$. If the domain walls all have roughly the same width $\lambda$, then the total volume of the domain walls scales as $\lambda A \sim t^{-n}$. Therefore, the contribution of the domain walls to any extensive property of the system would also be expected to scale as $t^{-n}$.

A gyroid is a minimal surface, so one would expect the contribution to the average squared curvature of the system from the well-formed gyroid regions inside domains to be small. On the other hand, the domain walls are non-gyroidal, and have non-zero mean curvature; if there is a roughly constant contribution to $\langle H^2 \rangle$ per unit volume of domain wall, then $\langle H^2 \rangle$ could also be expected to scale as $t^{-n}$. If this is the case, then that would further suggest that the length-scale of the gyroid domains indeed scales as $L \sim t^{1/2}$, indicative of random-walk or diffusive behaviour.
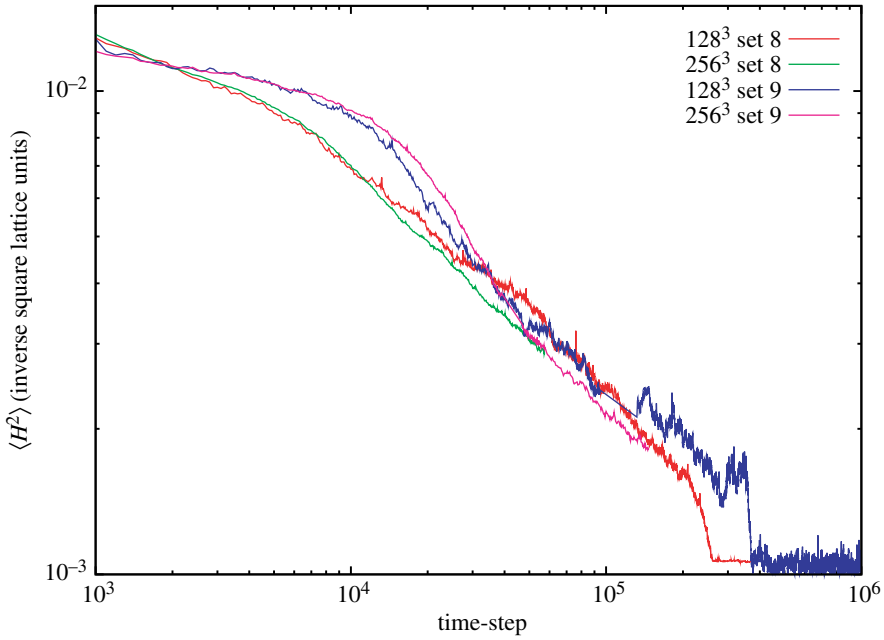
Figure 8. Averaged squared curvature against time for four simulations of different sizes and parameter sets. Late-time finite-size effect behaviour is clear in the $128^3$ simulations, where the curvature drops close to zero as a perfect minimal surface is formed.
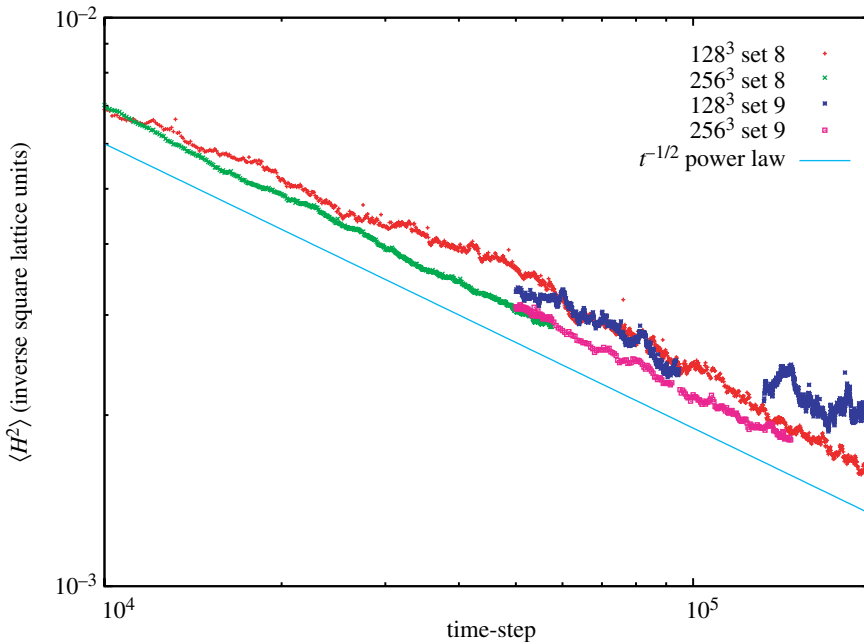


Figure 9. Averaged squared curvature in the power-law scaling régime for two parameter sets and sizes, with a $t^{-1/2}$ power law plotted as a guide to the eye.
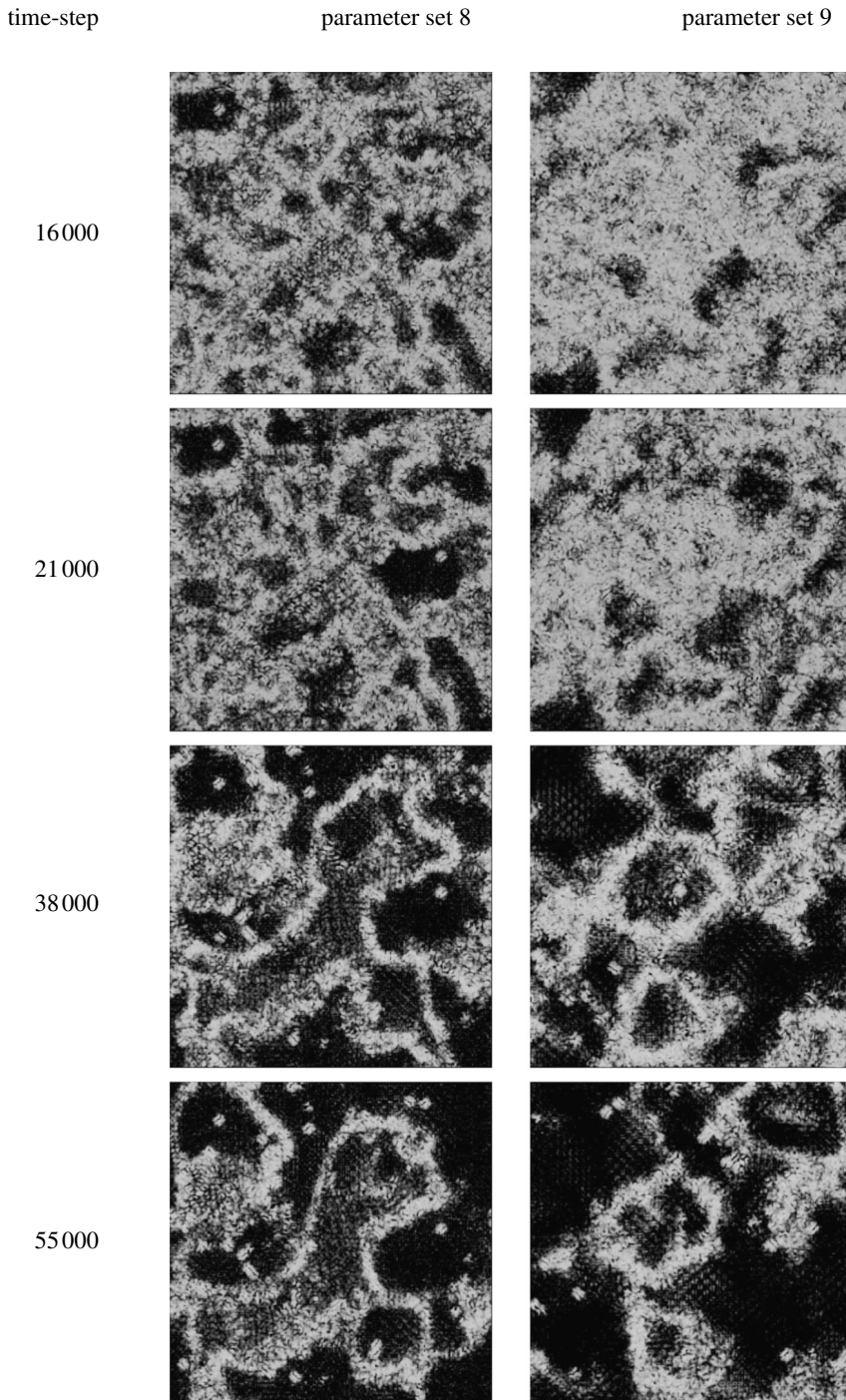
| time-step | parameter set 8 | parameter set 9 |
|-----------|-----------------|-----------------|

16 000

21 000

38 000

55 000

Figure 10. Volume rendering of domain walls in two $256^3$ systems. At earlier times, the parameter set 9 system has a larger density of defective, non-gyroidal regions. By time-step 55 000, both systems are much more clearly separated into domains.
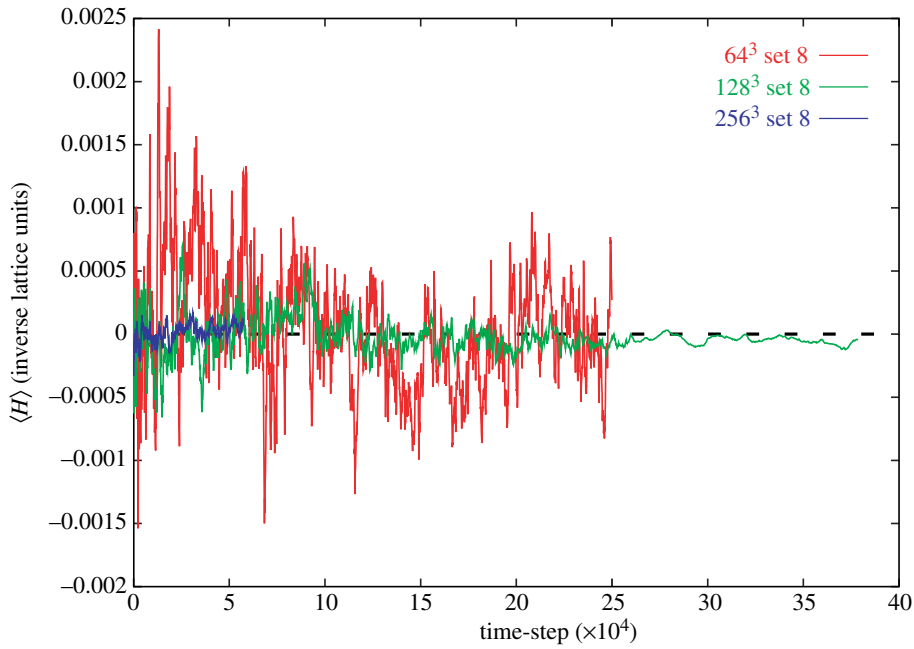
Figure 11. Mean curvature $H$ averaged over the $\phi=0$ surface for parameter set 8, for three different simulation sizes, showing that the fluctuation in mean curvature is reduced with system size.
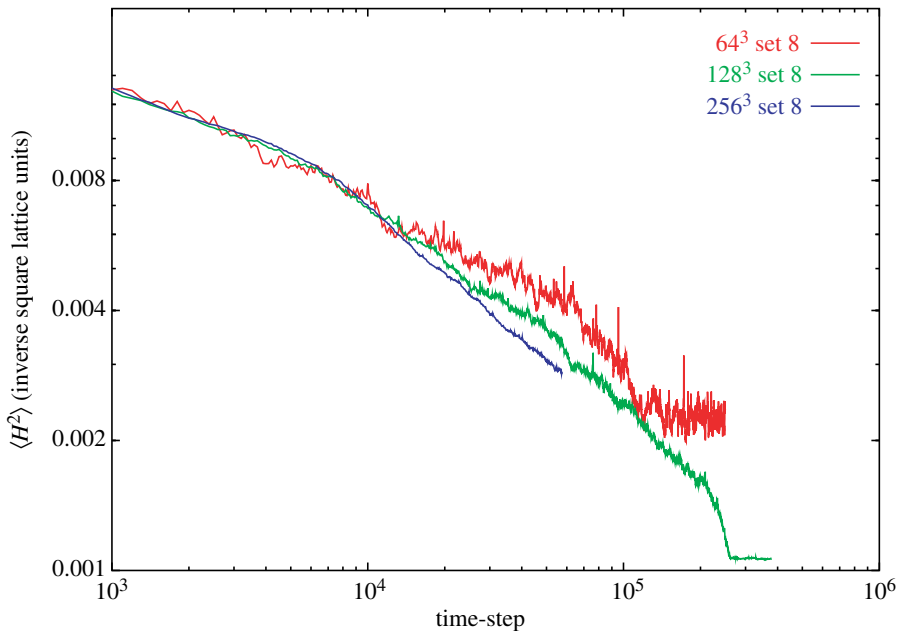
Figure 12. Squared mean curvature $H^2$ averaged over the $\phi=0$ surface for parameter set 8, showing smaller fluctuations in larger systems, and perfect minimal surface formation in the $128^3$ simulation.
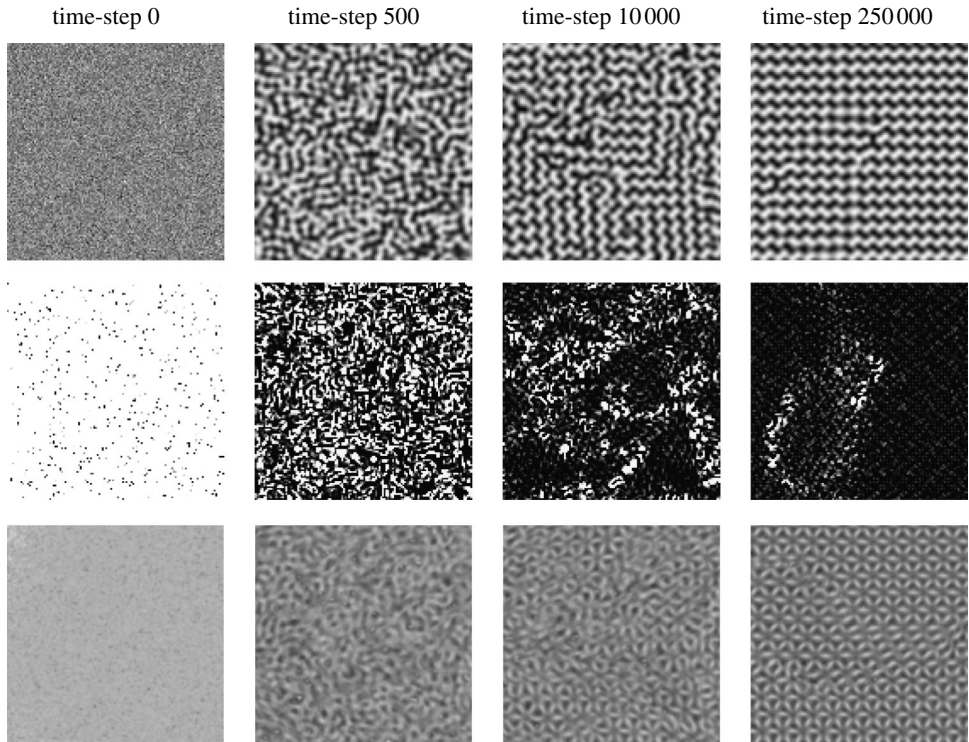
Figure 13. Images from a gyroid self-assembly simulation. The images in the top row show slices through the order parameter field, with oil-majority regions in black and water-majority regions in white. Images in the middle row show the corresponding interfacial curvature per lattice site, with high curvature white and low curvature black. Images in the bottom row show an orthographic-projection volume rendering of the order parameter, looking down the (111) direction to show the characteristic 'wagon wheel' pattern seen in electron micrographs (Thomas *et al.* 1988). The simulation was performed on a $128^3$ lattice using parameter set 8.

Table 3. Exponents $n$ for the relation $\langle H^2 \rangle = at^n$ fitted to the squared mean curvature of four simulations between the times $t_{\min}$, when clear domains have formed, and $t_{\max}$, when the finite size of either the system or the available computer resources limits the simulation.

| system | $t_{\min}$ | $t_{\max}$ | exponent ($\pm$ uncertainty in fit) |
|---|---|---|---|
| $128^3$ set 8 | 10 000 | 200 000 | $-0.474 \pm 0.001$ |
| $128^3$ set 9 | 50 000 | 300 000 | $-0.423 \pm 0.002$ |
| $256^3$ set 8 | 10 000 | 57 500 | $-0.5078 \pm 0.0008$ |
| $256^3$ set 9 | 50 000 | 146 500 | $-0.519 \pm 0.002$ |

# 8. Conclusions

Simulations of the self-assembly of a surfactant gyroid mesophase were performed; for the first time, the simulations were sufficiently large to clearly show the formation and evolution of multiple gyroid domains.

All systems underwent a rapid phase separation, during which oil and water phases formed a network of channels, separated by surfactant. After the phase separation, the systems began to form a gyroid mesophase. At late times, when clear domain walls had formed, power-law scaling of the average squared mean curvature of the system was observed, with exponent close to $-1/2$. This may indicate diffusive scaling of the length-scale of the domains themselves.

Analysis of simulated mesophases is non-trivial, due to the difficulty of defining a gyroid order parameter. In a ferromagnetic system, one can use the magnetization $\boldsymbol{M}(\boldsymbol{x})$ as an order parameter; all points within a ferromagnetic domain will have the same value of $\boldsymbol{M}$. In an ordinary fluid phase transition such as spinodal decomposition, the density of one fluid at a point can be subtracted from the density of the other, and normalized to give a scalar order parameter which varies from $+1$ in one fluid to $-1$ in the other, and which is zero in disordered, mixed regions. This kind of localized order parameter is sufficient to characterize the rapid separation of components before a mesophase is formed; however, after the initial demixing, further ordering of the system is morphological in nature, as gyroid regions are formed. Such a localized order parameter cannot describe this sort of ordering, since it is defined on too small a length-scale, and is not morphological in nature.

A set of tools was developed for calculating a polygonal approximation to the $\phi = 0$ surface of a simulated mesophase, in a topologically consistent manner; calculations of useful quantities such as the topologically invariant Euler characteristic, total interfacial area and interfacially averaged squared mean curvature were then possible. The average squared mean curvature was observed to vary as a power law with exponent approximately $-1/2$ over the régime where domains are clearly formed but finite-size effects have not yet set in; this may indicate random-walk motion of the domain walls. Direct visualization of the interface shows the existence of chiral domains, as should perhaps be expected for a symmetric amphiphile which has no intrinsic chirality. Once domains effectively disappeared due to reaching the simulation system size, the formation of line dislocations analogous to those in solid crystals was observed.

These simulations have opened up several avenues for further work. Even disregarding the physics involved, the techniques for characterization of lyotropic liquid crystal phases could still be improved, by looking at, for example, localized contributions to the interfacial curvature or Euler characteristic. Gyroid domain walls were observed to have a high density of points where both the local order parameter $\phi$ and the local order parameter gradient were small; while this may be due to the structure of the $\phi = 0$ surface inside domain walls, an improvement of this technique beyond a simple visual tool could lead to an algorithm for spatial localization of domain walls, and, consequently, the ability to make more quantitative analyses of the domain behaviour.

The simulations raise a number of physical questions. Those performed so far have all had 'oil'/'water' symmetry and a symmetric amphiphile, a situation which may be hard to realize exactly in experiment. The simulations produced chiral domains; it would be interesting to see if these could ever be produced experimentally, since the existence of such domains would affect the feasibility of producing gyroidal chirally selective filters. Observations of gyroid chirality

1079 would be difficult to make using TEM or SAXS techniques, but might be possible
1080 using, for example, transmission electron microtomography (Laurer *et al.* 1997).
1081   Finally, it is interesting to note that the lattice Boltzmann method allowed the
1082 bridging of two different length-scales in these simulations: the scale (approx. five
1083 lattice sites) of the single-fluid-component domains, and the scale (greater than
1084 or approx. 50 lattice sites) of gyroid domains.

1092

1093 # References
1094 Q14

1095 Armstrong, M. A. 1997 *Basic topology.* New York, NY: Springer. ISBN 0387908390.
1096 Avgeropoulos, A., Dair, B. J., Hadjichristidis, N. & Thomas, E. L. 1997 The tricontinuous double
1097   gyroid cubic phase in triblock copolymers of the ABA-type. *Macromolecules* **30**, 5634–5642.
1098   (doi:10.1021/ma970266z)
1099 Boghosian, B. M., Coveney, P. V. & Emerton, A. N. 1996 A lattice gas model of microemulsions.
1100   *Proc. R. Soc. A* **452**, 1221–1250.
1101 Bray, A. J. 1994 Theory of phase ordering kinetics. *Adv. Phys.* **43**, 357–459. (doi:10.1080/
1102   00018739400101505)
1103 Canham, P. B. 1970 The minimum energy of bending as a possible explanation of the biconcave
Q15   shape of the human red blood cell. *J. Theor. Biol.* **26**, 61–81.
1104 Carneiro, B. P., Silva, C. T. & Kaufman, A. E. 1996. Tetracubes: an algorithm to generate 3d
1105 Q16   isosurfaces based upon tetrahedral. In *Anais do IX SIBGRAPI*, pp. 205–210.
1106 Chan, V. Z. H., Hoffman, J., Lee, V. Y., Iatrou, H., Avgeropoulos, A., Hadjichristidis, N., Miller,
1107   R. D. & Thomas, E. L. 1999 Ordered bicontinuous nanoporous and nanorelief ceramic films
1108   from self assembling polymer precursors. *Science* **286**, 1716–1719. (doi:10.1126/science.286.
1109   5445.1716)
1110 Chen, H., Boghosian, B. M., Coveney, P. V. & Nekovee, M. 2000 A ternary lattice Boltzmann
Q17   model for amphiphilic fluids. *Proc. R. Soc. A* **456**, 2043–2057. (doi:10.1098/rspa.2000.0601)
1111 Chernyaev, E. V. 1995 Marching cubes 33: construction of topologically correct isosurfaces. Cern
1112   technical report cn 95-17, CERN.
1113 Chin, J. & Coveney, P. V. 2002 Lattice Boltzmann study of spinodal decomposition in two
1114 Q18   dimensions. *Phys. Rev. E* **66**.
1115 Cline, H. E., Lorensen, W. E., Ludke, S., Crawford, C. R. & Teeter, B. C. 1988 Two algorithms for
1116   the three-dimensional construction of tomograms. *Med. Phys.* **15**, 289–424. (doi:10.1118/
1117   1.596225)
1118 Coveney, P. V. & Skår, J. 2003 Developmental and physiological circuits: dissecting complexity.
1119   A report on a talk given by Dr Leroy Hood. *Phil. Trans. R. Soc. A* **361**, 1313–1317. (doi:10.
1120 Q19   1098/rsta.2003.1203)
1121 Czeslik, C. & Winter, R. 2002 Structure of water confined in the gyroid cubic phase of the lipid
1122   monoelaidin. *J. Mol. Liq.* **98**, 283–291. (doi:10.1016/S0167-7322(01)00332-4)
1123 Donnay, G. & Pawson, D. L. 1969 X-ray diffraction studies of echinoderm plates. *Science* **166**,
1124   1147–1150.
1125 Enlow, J. D., Enlow, R. L., McGrath, K. M. & Tate, M. W. 2004 Modelling liquid crystal bilayer
Q20   structures with minimal surfaces. *J. Chem. Phys.* **120**, 1981–1989. (doi:10.1063/1.1635811)
1126 Feynman, R. P., Leighton, R. B. & Sands, M. 1964 *The Feynman lectures on physics*, vol. 2.
1127   Reading, MA: Addison-Wesley. ISBN 0-201-02118-8.

Fogden, A. & Hyde, S. T. 1999 Continuous transformations of cubic minimal surfaces. *Eur. Phys. J. B* **7**, 91–104. (doi:10.1007/s100510050592)

Gandy, P. J. F. & Klinowski, J. 2000 Exact computation of the triply periodic G ('gyroid') minimal surface. *Chem. Phys. Lett.* **321**, 363–371. (doi:10.1016/S0009-2614(00)00373-0)

Gerig, G., Koller, T., Székely, G., Brechbuhler, C. & Kubler, O. 1999 Symbolic description of 3d structures applied to cerebral vessel tree obtained from MR angiography volume data. In *Information processing in medical imaging IPMI '93* (ed. H. H. Barrett & A. F. Gmitro), Lecture Notes in Computer Science, no. 687, pp. 94–111. New York, NY: Springer.

Gompper, G. & Schick, M. 1990 Correlation between structural and interfacial properties of amphiphilic systems. *Phys. Rev. Lett.* **65**, 1116–1119. (doi:10.1103/PhysRevLett.65.1116)

Gompper, G. & Schick, M. 1994 Self-assembling amphiphilic systems. In *Phase transitions and critical phenomena*, vol. 16 (ed. C. Domb & J. Lebowitz), pp. 1–176. London, UK: Academic Press.

González-Segredo, N. & Coveney, P. V. 2004*a* Coarsening dynamics of ternary amphiphilic fluids and the self-assembly of the gyroid and sponge mesophases: lattice-Boltzmann simulations. **Q21** *Phys. Rev. E* **69**. (doi:10.1103/PhysRevE.69.061501)

González-Segredo, N. & Coveney, P. V. 2004*b* Self-assembly of the gyroid cubic mesophase: lattice-Boltzmann simulations. *Europhys. Lett.* **65**, 795–801. (doi:10.1209/epl/i2003-10129-8)

González-Segredo, N., Nekovee, M. & Coveney, P. V. 2003 Three-dimensional lattice-Boltzmann simulations of critical spinodal decomposition in binary immiscible fluids. *Phys. Rev. E* **67**. **Q22** (doi:10.1103/PhysRevE.67.046304)

Goos, J. & Gompper, G. 1993 Topological defects in lamellar phases: passages and their fluctuations. *J. Phys. I France* **3**, 1551–1567. (doi:10.1051/jp1:1993200)

Góźdź, W. & Hołyst, R. 1996 High genus periodic gyroid surfaces of nonpositive Gaussian curvature. *Phys. Rev. Lett.* **76**, 2726–2729. (doi:10.1103/PhysRevLett.76.2726)

Große-Brauckmann, K. 1997 Gyroids of constant mean curvature. *Exp. Math.* **6**, 33–50.

Groot, R. D. & Madden, T. J. 1998 Dynamic simulation of diblock copolymer microphase separation. *J. Chem. Phys.* **108**, 8713–8724. (doi:10.1063/1.476300)

Grotberg, J. B. & Gaver, D. P. 1996 A synopsis of surfactant spreading research. *J. Colloid Interface Sci.* **178**, 377–378. (doi:10.1006/jcis.1996.0130)

Hajduk, D. A., Harper, P. E., Gruner, S. M., Honeker, C. C., Kim, G., Thomas, E. L. & Fetters, L. J. 1994 The gyroid—a new equilibrium morphology in weakly segregated diblock copolymers. *Macromolecules* **27**, 4063. (doi:10.1021/ma00093a006)

Hołyst, R. & Oswald, P. 1998 Confined complex liquids: passages, droplets, permanent deformations, and order–disorder transitions. *J. Comp. Phys.* **109**, 11 051–11 060.

Hyde, S. T. 1989 The microstructure of bicontinuous surfactant aggregates. *J. Phys. Chem.* **93**, 1458–1464. (doi:10.1021/j100341a055)

Hyde, S. T. & Ramsden, S. 2000 Polycontinuous morphologies and interwoven helical networks. *Europhys. Lett.* **50**, 135–141. (doi:10.1209/epl/i2000-00245-y)

Hyde, S. T. & Schroeder, G. E. 2003 Novel surfactant mesostructural topologies: between lamellae and columnar (hexagonal) forms. *Curr. Opin. Colloid Interface Sci.* **8**, 5–14. (doi:10.1016/S1359-0294(03)00014-1)

Karcher, H. & Polthier, K. 1996 Construction of triply periodic minimal surfaces. *Phil. Trans. R. Soc. A* **354**, 2077–2104.

Kendon, V. M., Desplat, J. C., Bladon, P. & Cates, M. E. 1999 3D spinodal decomposition in the inertial regime. *Phys. Rev. Lett.* **83**, 576–579. (doi:10.1103/PhysRevLett.83.576)

Kinsey, L. C. 1993 *Topology of surfaces*. New York, NY: Springer. ISBN 0387941029.

Kittel, C. 1996 *Introduction to solid state physics*, 7th edn. Chichester, UK: Wiley. ISBN 0-471-11181-3.

Klinowski, J., Mackay, A. L. & Terrones, H. 1996 Curved surfaces in chemical structure. *Proc. R.* **Q23** *Soc. A* **364**, 1975–1987.

Lamura, A., Gonnella, G. & Yeomans, J. M. 1999 A lattice Boltzmann model of ternary fluid mixtures. *Europhys. Lett.* **45**, 314–320. (doi:10.1209/epl/i1999-00165-4)

Landh, T. 1995 From entangled membranes to eclectic morphologies: cubic membranes as subcellular space organizers. *FEBS Lett.* **369**, 13–17. (doi:10.1016/0014-5793(95)00660-2)

**Q24** Langevin, D. 1999 *Europhysics News*, 72–73.

Laurer, J. H., Hajduk, D. A., Fung, J. C., Sedat, J. W., Smith, S. D., Gruner, S. M., Agard, D. A. & Spontak, R. J. 1997 Microstructural analysis of a cubic bicontinuous morphology in a neat SIS triblock copolymer. *Macromolecules* **30**, 3938. (doi:10.1021/ma970449l)

Lewiner, T., Lopes, H., Vieira, A. W. & Tavares, G. 2003 Efficient implementation of marching cubes cases with topological guarantees. *J. Graphics Tools* **8**, 1–15.

Lord, E. A. & Mackay, A. L. 2003 Periodic minimal surface of cubic symmetry. *Curr. Sci.* **85**, 346–362.

Lorensen, W. E. & Cline, H. E. 1987 Marching cubes: a high resolution 3d surface construction algorithm. *Comput. Graphics* **21**, 163–169.

Love, P. J., Coveney, P. V. & Boghosian, B. M. 2001 Three-dimensional hydrodynamic lattice-gas simulations of domain growth and self assembly in binary immiscible and ternary amphiphilic

**Q25** fluids. *Phys. Rev. E* **64**.

Mackay, A. L. 1985 Periodic minimal surfaces. *Nature* **314**, 604–606. (doi:10.1038/314604a0)

Mariani, P., Paci, B., Bösecke, P., Ferrero, C., Lorenzen, M. & Caciuffo, R. 1996 Effects of hydrostatic pressure on the monoolein–water system: an estimate of the energy function of the inverted *Ia3d* cubic phase. *Phys. Rev. E* **54**, 5840–5843. (doi:10.1103/PhysRevE.54.5840)

Nakahara, M. 1993 *Geometry, topology, and physics*, 2nd edn. Bristol, UK: IOP Publishing. ISBN 0852740956.

Nekovee, M. & Coveney, P. 2001 Lattice-Boltzmann simulations of self-assembly of a binary water–surfactant system into ordered bicontinuous cubic and lamellar phases. *J. Am. Chem. Soc.* **123**, 12 380–12 382. (doi:10.1021/ja015555o)

Nissen, H.-U. 1969 Crystal orientation and plate structure in echinoid skeletal units. *Science* **166**, 1150–1152.

Patton, J. S. & Carey, M. C. 1979 Watching fat digestion. *Science* **204**, 145–148.

Pickles, S. M. *et al.* 2004 The TeraGyroid experiment. In *Proc. Workshop on Case Studies on Grid Applications at GGF 10, Berlin, Germany, 13 March 2004* (ed. T. Hinke, S. J. Cox, R. T. Hood

**Q26** & J. Towns).

Prestegard, J. H. & O'Brien, M. P. 1987 Membrane and vesicle fusion. *Annu. Rev. Phys. Chem.* **38**, 383–411. (doi:10.1146/annurev.pc.38.100187.002123)

Prinsen, P., Warren, P. B. & Michels, M. A. J. 2002 Mesoscale simulations of surfactant dissolution and mesophase formation. *Phys. Rev. Lett.* **89**, 148 302. (doi:10.1103/PhysRevLett.89.148302)

Rand, R. P. 1981 Interacting phospholipid bilayers: measured forces and induced structural changes. *Annu. Rev. Biophys. Bioeng.* **10**, 277–314. (doi:10.1146/annurev.bb.10.060181.001425)

Rigler, M. W., Honkanen, R. E. & Patton, J. S. 1986 Visualization by freeze fracture, *in vitro* and *in vivo* of the products of fat digestion. *J. Lipid Res.* **27**, 836–857.

Rybka, R. B., Cieplak, M. & Salin, D. 1995 Boltzmann cellular automata studies of the spinodal decomposition. *Physica A* **222**, 105–118. (doi:10.1016/0378-4371(95)00209-X)

Sakurai, S., Umeda, H., Furukawa, C., Irie, H., Nomura, S., Lee, H. H. & Kim, J. K. 1998 Thermally induced morphological transition from lamella to gyroid in a binary blend of diblock copolymers. *J. Chem. Phys.* **108**, 4333–4339. (doi:10.1063/1.475834)

Schoen, A. 1970 Infinite periodic minimal surfaces without self-intersections. *NASA Tech. Note*, D-5541, Washington, DC.

Schröder, G. E., Ramsden, S. J., Fogden, A. & Hyde, S. T. 2004 A rhombohedral family of minimal surfaces as a pathway between the P and D cubic mesophases. *Physica A* **339**, 137–144. (doi:10.1016/j.physa.2004.03.056)

Schwarz, U. S. & Gompper, G. 1999 A systematic approach to bicontinuous cubic phases in ternary amphiphilic systems. *Phys. Rev. E* **59**, 5528–5541. (doi:10.1103/PhysRevE.59.5528)

Schwarz, U. S. & Gompper, G. 2000 Stability of inverse bicontinuous cubic phases in lipid–water mixtures. *Phys. Rev. Lett.* **85**, 1472–1475. (doi:10.1103/PhysRevLett.85.1472)

Schwarz, U. & Gompper, G. 2002 *Bicontinuous surfaces in self-assembling amphiphilic systems*, vol. 600 of Springer Lecture Notes in Physics, pp. 107–151. New York, NY: Springer.

Scriven, L. E. 1976 Equilibrium bicontinuous structure. *Nature* **263**, 123–125. (doi:10.1038/263123a0)

Scriven, L. E. & Sternling, C. V. 1960 The Marangoni effects. *Nature* **187**, 186–188.

Seddon, J. M. & Templer, R. H. 1993 Cubic phases of self-assembled amphiphilic aggregates. *Phil. Trans. R. Soc. A* **344**, 377–401.

Seddon, J. M. & Templer, R. H. 1995 Polymorphism of lipid–water systems. In *Handbook of biological physics* (series ed. A. J. Hoff). *Structure and dynamics of membranes*, vol. 1 (ed. R. Lipowsky & E. Sackmann), ch. 3, pp. 97–160. Amsterdam, The Netherlands: Elsevier.

Shefelbine, T. A., Vigild, M. E., Matsen, M. W., Hajduk, D. A., Hillmyer, M. A., Cussler, E. L. & Bates, F. S. 1999 Core-shell gyroid morphology in a poly(isoprene-*block*-styrene-*block*-dimethylsiloxane) triblock copolymer. *J. Am. Chem. Soc.* **121**, 8457–8465. (doi:10.1021/ja991442h)

Stier, A., Finch, S. A. E. & Bösterling, B. 1978 Non-lamellar structure in rabbit liver microsomal membranes: a 31P-NMR study. *FEBS Lett.* **91**, 109–112. (doi:10.1016/0014-5793(78)80028-3)

Theissen, O., Gompper, G. & Kroll, D. M. 1998 Lattice-Boltzmann model of amphiphilic systems. *Europhys. Lett.* **42**, 419–424. (doi:10.1209/epl/i1998-00265-7)

Thomas, E. L., Anderson, D. M., Henkee, C. S. & Hoffman, D. 1988 Periodic area minimizing surfaces in block copolymers. *Nature* **334**, 598–601. (doi:10.1038/334598a0)

Treece, G. M., Prager, R. W. & Gee, A. H. 1999 Regularised marching tetrahedra: improved iso-surface extraction. *Comput. Graphics* **23**, 583–598. (doi:10.1016/S0097-8493(99)00076-X)

Urbas, A. M., Maldovan, M., DeRege, P. & Thomas, E. L. 2002 Bicontinuous cubic block copolymer photonic crystals. *Adv. Mater.* **14**, 1850–1853. (doi:10.1002/adma.200290018)

Velasco, E. & Toxvaerd, S. 1993 Computer simulation of phase separation in a two-dimensional binary fluid mixture. *Phys. Rev. Lett.* **71**, 388–391. (doi:10.1103/PhysRevLett.71.388)

Wagner, A. J. & Yeomans, J. M. 1998 Breakdown of scale invariance in the coarsening of phase-separating binary fluids. *Phys. Rev. Lett.* **80**, 1429–1432. (doi:10.1103/PhysRevLett.80.1429)

## Author Queries

Q1   Please check the edit of the value '057500' to '57500' in table 3.
Q2   Please define the term '[p]' given in table 3.
Q3   Please check the change in short title as the given short title exceeds the maximum length (40 characters) normally permitted.
Q4   Please supply a minimum of three to a maximum of six keywords.
Q5   Please check the edit of the word 'nett' to 'net'.
Q6   In the following sentence 'The gyroid has symmetry group Ia3d', please confirm whether it should be 'The gyroid has space group symmetry Ia3d'.
Q7   Please provide the expansion of the term 'DPD'.
Q8   In the following sentence '...a membrane spanning both the x and y directions...' should 'x' and 'y' be in upper case? Please clarify.
Q9   Please define the acronym 'MRI'.
Q10  In the following sentence 'The following section presents the actual analysis of the generated data...' can it be changed to read as 'The following sections present the actual analysis of the generated data...'. Please confirm.
Q11  Please check the inserted citation of figure 5 so that the citations are in order.
Q12  Please check the inserted citation of figures 8–10 so that the citations are in order.
Q13  In the following sentence 'Both of the parameter set 8 systems...' please clarify whether the word 'both' refers to sets 8 and 9.
Q14  Please check the inserted article title for all journal references.
Q15  Please check the initials of the author 'Canham' in reference Canham (1970). Should it be 'P.'?
Q16  Please provide editor name(s)/initial(s), publisher's name and location for reference Carneiro et al. (1996).
Q17  Please check whether the last page number '2047' should be '2057' in reference Chen et al. (2000).
Q18  Please provide page range for reference Chin & Coveney (2002).
Q19  Please check the edit of the volume number '261' to '361' in reference Coveney & Skår (2003).
Q20  Please check the edit of the journal title 'J. Comp. Phys.' to 'J. Chem. Phys.' in references Enlow et al. (2004) and Groot & Madden (1998).
Q21  Please provide page range for reference González-Segredo & Coveney (2004a).
Q22  Please provide page range for reference González-Segredo et al. (2003).
Q23  Please check the details in reference Klinowski et al. (1996).
Q24  Please provide article title and volume number for reference Langevin (1999).
Q25  Please provide page range for reference Love et al. (2001).
Q26  Please provide page range, publisher's name and the town of publication for reference Pickles et al. (2004).